High Temperature Corrosion of Materials (2026) 103:75
https://doi.org/10.1007/s11085-026-10435-w

REVIEW

A Unifying Review of Breakaway Oxidation in Early Transition Metals at High Temperatures

Isha Gupta[1] · **Shalini Tripathi**[2] · **B. Gorr**[3]

Received: 5 May 2026 / Revised: 30 June 2026 / Accepted: 4 July 2026

Abstract

Early transition metals from Groups IV to VI are critical for maintaining structural integrity at high temperatures. However, their performance is often limited by breakaway oxidation, the transition from initially protective oxide growth to accelerated, non-protective oxidation. Despite decades of research, the underlying mechanisms remain unresolved, even within individual metals. This review argues that the shared oxidation characteristics of these metals warrant a unified assessment to constrain the mechanistic space and guide focused future studies. Experimental and theoretical evidence across Ti, Zr, Nb, Ta, and W is synthesized to identify critical gaps in current understanding. This unified perspective suggests that breakaway may arise from coupled instabilities at the metal-oxide interface involving oxygen dissolution into the metal, defect-rich monoxides, and growth-induced stresses that promote cracking and porosity. In addition, alloying and processing strategies proposed to enhance the oxidation resistance of these metals are synthesized. Finally, the influence of early transition metals on the oxidation performance of emerging refractory high-entropy alloys is discussed, highlighting the broader significance of the mechanistic insights developed in this review. These insights are particularly timely given the urgent demand for oxidation-resistant materials in ultra-high temperature applications.

Keywords Breakaway oxidation · Early transition metals · Refractory metals · Oxide scales · High-temperature oxidation

✉ Isha Gupta
isha.gupta@soton.ac.uk

[1] Department of Aeronautics and Astronautics, University of Southampton, Southampton, UK

[2] Pacific Northwest National Laboratory, Richland, WA, USA

[3] Karlsruhe Institute of Technology, Institute for Applied Materials – Applied Materials Physics, Karlsruhe, Germany

Published online: 20 July 2026

Introduction

As demand for higher operating temperatures grows in aerospace and energy sectors, reliable high-temperature structural materials are increasingly critical. Early transition metals from Groups IV, V, and VI, such as Ti, Zr, Hf, V, Nb, Ta, Mo, and W, play a crucial role in these applications. Ti alloys provide lightweight, high-strength components for aircraft engines [1], while Zr-based alloys are widely used as nuclear fuel cladding [2]. A subset of these metals from Groups V and VI belongs to the refractory class (e.g., Nb, Mo, Ta, W, and V). These materials are the leading candidates for ultra-high temperature structural applications, including next-generation hypersonic vehicles [3] and advanced nuclear reactors [4–6].

Recently, refractory multi-principal element alloys (RMPEA) and refractory high-entropy alloys (RHEA) have gained significant interest for applications beyond the capabilities of Ni-based superalloys [7–11]. While early alloy designs consisted of only the refractory elements, subsequent compositions include a broader range of elements drawn from Groups IV–VI to improve material properties, in particular plasticity and density [7, 12]. However, rapid oxidation of most RMPEA and RHEA remains a major drawback, limiting their potential as next-generation high-temperature alternatives to Ni-based superalloys [10, 13–16].

The oxidation performance of early transition metals, especially refractory metals, is limited by the porous, cracked, and volatile nature of the oxide scales that form on them [4, 7, 13, 17–19]. While a passive and adherent oxide layer slows oxidation over time (typically following parabolic kinetics), oxides formed on these metals often deviate from this ideal. Formation of volatile oxides can lead to rapid mass loss. In contrast, morphological degradation such as oxide cracking, porosity, scale spallation, or layered oxide formation can promote accelerated oxidation kinetics. This kinetic acceleration is typically referred to as breakaway oxidation. Both processes compromise structural integrity and limit component lifetime.

Oxide volatilization can be predicted relatively easily through thermodynamic considerations (e.g., in Mo above 750 °C and in W above 1000 °C). Breakaway oxidation, however, arises from a complex interplay of mechanical, thermodynamic, and kinetic processes that degrade the oxide scale and ultimately undermine its protectiveness.

In this review, the term breakaway is used broadly to denote any transient or sustained departure from ideal protective parabolic weight-gain kinetics that accelerates oxidation. The term linear breakaway refers specifically to a sustained departure to approximately linear kinetics. Typical oxidation behaviors associated with breakaway in early transition metals and their alloys are shown schematically in Fig. 1. These behaviors can be grouped into three broad categories: d irect linear breakaway (pure Nb, Ta, Zr); periodic kinetic transitions followed by linear breakaway (Zr alloys); and weak transients followed by linear breakaway (pure Ti, W). These kinetic definitions are distinguished from the morphological degradation processes which contribute to the underlying loss of oxide protectiveness.

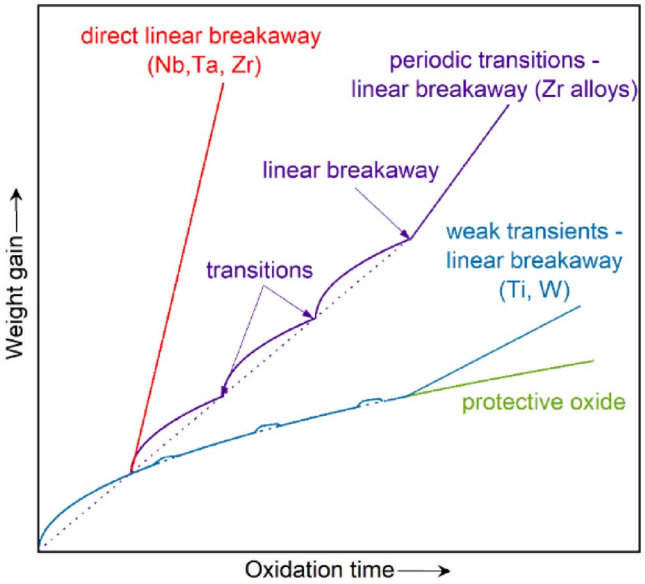

Fig. 1 Schematics of typical oxidation kinetics associated with breakaway in early transition metals and their alloys [2, 4, 17, 19–24]. Breakaway is used here as a broad term for departures from protective parabolic kinetics that accelerate oxidation; linear breakaway refers specifically to a sustained departure to approximately linear kinetics

Breakaway oxidation behaviors in early transition metals have been reported for more than 50 years [25–28]. Much of the mechanistic insights stem from Zr alloys due to their widespread use as nuclear fuel cladding [2, 29]. In contrast, metals such as Ta and Nb have seen little modern investigation, with most studies dating back to the 1960–1990s [17, 19, 20, 24, 30, 31].

Despite these efforts, a comprehensive understanding of the underlying mechanisms and governing factors remains elusive [2, 28, 29, 32, 33]. Even in widely studied Zr alloys, the precise cause of oxide degradation is still debated [32, 34–38]. This largely material-specific literature provides a fragmented and often contradictory understanding of breakaway, with multiple distinct mechanisms proposed within individual materials. This gap motivates the unified assessment developed here, which is based on the shared oxidation characteristics reported across several early transition metals, including dominant anionic diffusion, large in-plane compressive growth stresses, multiphase oxide scales, and periodic oxide morphologies. Identifying potentially common factors associated with breakaway can provide a clearer direction for targeted future research.

This review critically examines the experimental and modeling evidence in Ti, Zr, Nb, Ta, and W to evaluate underlying mechanisms and identify a possible unifying framework for breakaway oxidation. These metals are selected as primary case studies because they provide the most complete evidence linking oxidation kinetics, oxide morphology, and mechanisms of oxide protectiveness loss. Because comparable mechanistic literature is lacking for Hf, V, and Mo, these metals are discussed only to assess the applicability of the proposed framework

beyond the primary systems, rather than as supporting evidence. In addition, oxidation of V and Mo may be dominated by volatile or low-melting oxides and subsequent mass loss [39, 40], whereas this review focuses on breakaway associated with an accelerated rate of weight gain due to the loss of oxide protectiveness.

The evidence base for the framework focuses primarily on pure metals to isolate fundamental processes from alloying effects. However, Zr alloys are included because they dominate the mechanistic literature and share key oxidation characteristics with pure early transition metals. The relevance of the proposed framework to emerging refractory high-entropy alloys, in which early transition metals are common constituents, is also discussed.

The present review is organized into the following sections.

Section 2: Mechanistic review of breakaway: Physical, thermodynamic, and kinetic processes driving oxide degradation; identifies potential unifying breakaway factors.

Section 3: Pre- and post-breakaway kinetics; breakaway conditions: Trends and shared mechanisms governing these regimes.

Section 4: Comparative assessment of oxidation behavior and breakaway evidence: Comparison of key oxidation features and breakaway evidence across Ti, Zr, Nb, Ta, and W.

Section 5: Breakaway models: State-of-the-art modeling approaches.

Section 6: Strategies to enhance the oxidation resistance: Key alloying and processing methods.

Section 7: Relevance to refractory high-entropy alloys (RHEAs): Influence of early transition metal oxidation on the performance of emerging RHEAs.

Section 8: Conclusions and outlook: Identifying key opportunities for future research.

Mechanistic Review of Breakaway

A wide range of mechanisms have been proposed to explain the loss of oxide protectiveness underlying the diverse breakaway behaviors in Ti, Zr, Nb, Ta, and W shown in Fig. 1. Summarized in Fig. 2, these mechanisms fall into three broad categories:

(a) Physical: Mechanical instabilities from the oxide growth stresses or metal-oxide interface morphology, which can induce cracking and create pathways for oxygen ingress.
(b) Thermodynamic: Phase evolution within the oxide that alters diffusion rates or generates stress fields that promote cracking.
(c) Kinetic: Diffusion or reaction processes which may drive pore formation or other instabilities that deviate from classical parabolic growth.

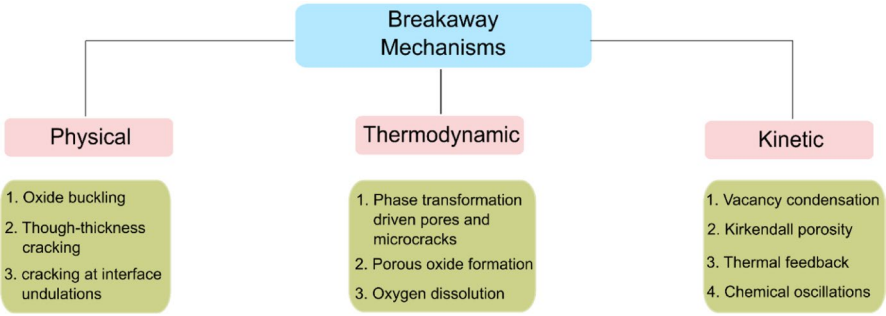

Fig. 2 Proposed mechanisms for the loss of oxide protectiveness associated with breakaway oxidation behaviors

Table 1 Shared oxidation features of Ti, Zr, Nb, Ta, and W and their potential influence on the proposed degradation mechanisms summarized in Fig. 2

Common feature	Description	Mechanistic influence
Anionic diffusion	Inward oxygen transport, often described as n-type oxygen-vacancy transport	Generates compressive growth stresses, linked to pore formation and defect-controlled phase transformations [37, 41, 42]
Compressive stresses within the oxide	Due to anionic diffusion and PBR > 1	Linked to oxide buckling, cracking near interface undulations, and stress-driven phase transformations [35, 36, 43]
Multiphase oxide scale	Enabled by multiple oxidation states	Linked to formation of porous higher-valence oxides and phase transformations that promote cracking and exfoliation [27, 44]

Shared Oxidation Characteristics

Although the mechanisms synthesized in Fig. 2 largely originate from individual material studies, they are governed by underlying processes that are common across Ti, Zr, Nb, Ta, and W, as highlighted in Table 1. The strong coupling between these shared features and the mechanisms proposed to cause the loss of oxide protectiveness motivates the need for a unified assessment.

Striking similarities in oxide morphologies observed across Ti, Zr, Nb, Ta, and W further support the unifying influence of features listed in Table 1. Layered or stratified oxides with periodically spaced void-like features are reported in Ti [33, 43, 45, 46], Zr [2, 32, 47, 48], Ta [4, 49–51], Nb [19, 50, 52], and W [21, 22] systems, as shown by representative micrographs in Fig. 3. In Zr alloys, these features correlate directly with periodic kinetic transitions, each of which nearly resets the oxidation kinetics to a new parabolic growth segment (Fig. 1). This behavior indicates a substantial loss of protectiveness in the preceding oxide layer [34, 53]. Limited studies on pure Zr also suggest formation of layered oxides [54–56]. In Ti and W, formation of new sub-layers instead produces weak periodic or irregular fluctuations while the overall kinetics remains parabolic (Fig. 1), suggesting that previous sub-layers retain partial protectiveness [20, 21, 57].

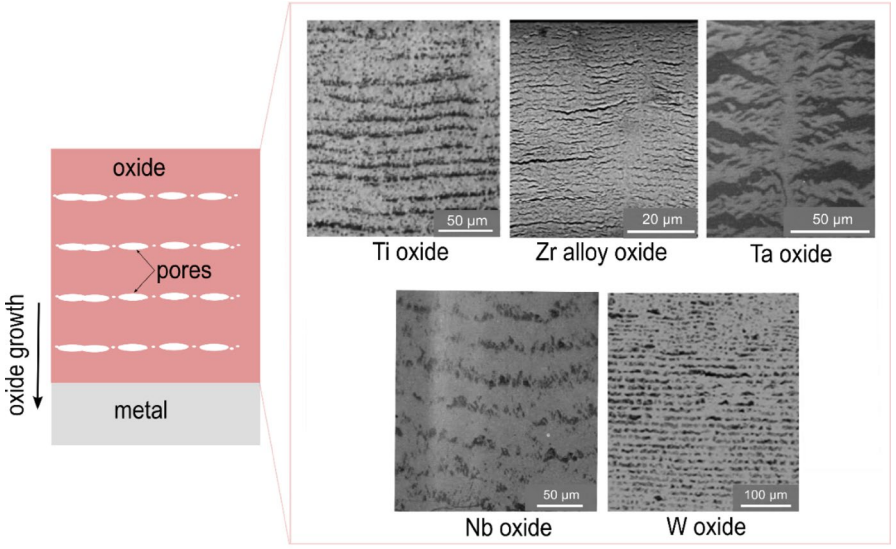

Fig. 3 Periodically layered oxide structures observed in Ti, Zr, Nb, Ta, and W, which may underlie the breakaway behaviors illustrated in Fig. 1. Source-study conditions are: pure Ti, 900 °C, moist air with dewpoint of 8 °C [59]; ZIRLO alloy, 415 °C, steam [47]; single-crystal Nb, 925 °C, 0.55 atm O_2 [52]; single-crystal Ta, 820 °C, 0.60 atm O_2 [49]; and 99.97% pure W, 700 °C, air [21]. These conditions correspond to the selected representative micrographs and should not be interpreted as limiting the occurrence of periodic layering to those conditions. The images of Ti, Ta, Nb, and W oxides are adapted from [59], [49], [52], and [21],respectively, with permission from Elsevier. The Zr alloy oxide image is adapted from Preuss et al., "Studies Regarding Corrosion Mechanisms inZirconium Alloys,"Journal of ASTM International 8(9) (2011), Fig. 1. Used with permission of ASTM International; permission conveyed throughCopyright Clearance Center, Inc. All images were cropped to highlight periodic layering, and scale bars were added after cropping

Layered oxide structures are also reported after the onset of linear breakaway across Ti, Zr, Nb, Ta, and W [19–22, 25, 26, 34]. This has led to the hypothesis that the apparent linear kinetics in this regime may consist of successive parabolic segments separated by kinetic transitions that become difficult to resolve due to non-uniform oxidation along the metal-oxide interface [19, 20, 25, 26, 34, 58]. In fast-oxidizing metals such as pure Nb, Ta, and Zr, this stage may begin early, giving the appearance of a direct linear breakaway without preceding periodic kinetic transitions (Fig. 1).

Taken together, these observations suggest spatiotemporal oxidation periodicity as an additional shared feature of these metals that may provide a basis for interpreting the diverse breakaway kinetic behaviors shown in Fig. 1.

These shared oxidation characteristics suggest that common mechanisms may contribute to breakaway in early transition metals. The following sections critically examine proposed physical, thermodynamic, and kinetic mechanisms and assess their potential universality. The literature often does not differentiate between mechanisms responsible for periodic kinetic transitions, weak transients, and linear breakaway, instead emphasizing factors that cause the underlying loss of oxide protectiveness. Because the post-linear-breakaway regime may itself consist of unresolved succes-

sive periodic transitions associated with periodic layering, this review focuses on identifying common degradation mechanisms rather than assessing each breakaway kinetic behavior separately.

Pure Zr Versus Zr Alloys

Because much of the mechanistic literature on breakaway comes from Zr alloys, the transferability of these observations to pure Zr and other early transition metals requires careful assessment. Mechanisms that depend specifically on alloying elements cannot be treated as directly applicable to pure Zr or to other early transition metals. Examples include alloying-element-influenced Kirkendall porosity and the tetragonal-to-monoclinic transformation in ZrO_2, both of which are identified in the discussion below as Zr-alloy-specific or composition-sensitive and are not generalized to pure metals.

At the same time, Zr alloys remain valuable mechanistic analogues because several oxidation characteristics central to this review are shared with pure early transition metals. These include anionic diffusion, large compressive growth stresses, and multiphase oxide scales [41, 42, 60–63]. In addition, periodic layering is reported across Zr alloys with different alloying additions and also has analogues in pure Zr, Ti, Nb, Ta, and W [54–56] (Fig. 3). Therefore, Zr-alloy studies are used here not as direct proof that identical mechanisms operate in pure early transition metals, but as evidence for degradation processes that may be relevant when they arise from shared oxidation characteristics rather than alloy-specific effects.

Physical Mechanisms

Early transition metals from Groups IV–VI exhibit a Pilling-Bedworth ratio (PBR) > 1 and oxidize primarily via anionic diffusion (except Cr), generating in-plane compressive stresses within the oxide [41, 42]. The presence of lateral pores or crack-like features associated with periodically layered oxides is well documented (Fig. 3), but their origin and mechanistic role remains debated. These features have been interpreted as cracks formed to relax the compressive growth stresses [21, 34, 64, 65]. However, their 3D characterization (Fig. 4) combined with a mechanics-based analysis in Zr alloys shows that such cracks are insufficient to induce buckling and spallation of the oxide layer, a necessary condition for stress relaxation [66]. Other studies instead attribute their origin to localized tensile stresses associated with metal-oxide interface undulations [35, 67–69].

How lateral pores enclosed within the oxide (Fig. 4) accelerate oxidation without spallation remains unclear. They may connect with vertical pores to create fast oxygen ingress pathways [2, 37, 70] ("Kinetic Mechanisms" Section). Other studies argue that the lateral porosity may instead be a sample-preparation artifact [28, 34, 48, 71], shifting attention to through-thickness cracking as the underlying mechanism. However, experiments and modeling preclude such cracks before the first kinetic transition in flat specimens [34, 42, 72].

Although direct evidence is largely limited to Zr alloys, shared oxidation characteristics highlighted in Table 1 suggest that periodically layered oxide morphologies

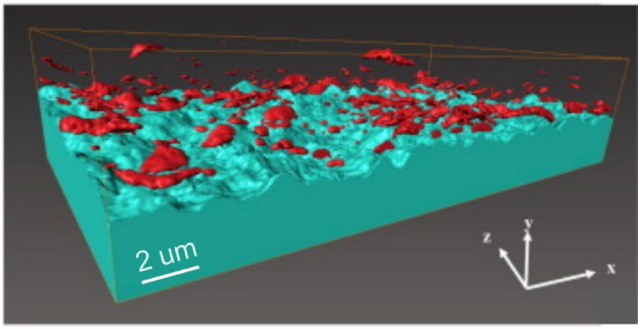

Fig. 4 3D morphology of lateral pores that separate periodic sublayers in the oxide grown on ZIRLO shortly after the first kinetic transition in oxidation kinetics. Red regions show pores embedded within the oxide and green region represents the substrate. Adapted from [66] with permission from Elsevier. A scale bar has been added

and associated breakaway behaviors (Figs. 1 and 3) cannot be explained by stresses alone. The absence of periodicity in thin substrates nevertheless suggests that stresses remain relevant [50]. A more plausible role is that stresses act indirectly by modifying phase stability, promoting defect accumulation, or influencing defect transport. These coupled effects may promote local pore or crack formation, metal fragmentation, or other disruptions to the oxide-scale stability, thereby contributing to the loss of protectiveness.

Thermodynamic Mechanisms

The presence of multiphase oxide scales is well established across Ti, Zr, Nb, Ta, and W. However, the strength of evidence linking specific phase changes to breakaway oxidation is system-specific. Proposed phase changes can be grouped into three categories: formation of higher-valence porous oxides, phase transformations within the principal oxide, and localized phase instabilities at the metal-oxide interface. Evidence from individual material studies is synthesized first, followed by a discussion of their potential universality.

Formation of Porous Oxides

Because transition metals exhibit multiple oxidation states, breakaway in some metals has been attributed to a transition from the formation of a compact, lower-valence oxide to a more porous, higher-valence oxide that can provide pathways for rapid oxygen ingress. Examples include transition from a suboxide (possibly, W_4O_{11}) to WO_3 [41, 44] in tungsten, and from NbO_2 to Nb_2O_5 [24] in niobium, where the latter is supported by XRD data. The porosity of higher-valence oxides may result from increased stresses associated with their larger molar volumes ("Physical Mechanisms" Section).

Phase Transformation Within the Principal Oxide

In Zr alloys, a tetragonal-to-monoclinic (T → M) martensitic transformation within the principal oxide scale (i.e., ZrO_2) has been proposed to promote microcracking, causing periodic kinetic transitions [36, 37, 73]. Supporting evidence includes synchrotron XRD data showing spatial periodicity in phase content, and reports of abrupt increases in transformation rate during periodic kinetic transitions [36, 74, 75]. However, other studies report no such periodicity or sudden transformations [47, 69, 76–79]. These discrepancies likely arise from variations in the alloy chemistry, oxidation conditions, and characterization methods.

Phase Instability at Metal-Oxide Interface

In Ta and Nb, metal exfoliation associated with oxygen dissolution into the metal and the formation of suboxides (e.g., TaO_z, NbO_z) have been linked to breakaway. These suboxides have been reported as platelet-like structures at the metal-oxide interface (Fig. 5). Strains associated with oxygen uptake or further oxidation of these suboxides have been proposed to induce metal exfoliation and promote breakaway [27, 52].

In Zr alloys, advanced characterization techniques such as electron energy-loss spectroscopy (EELS) and atom probe tomography (APT) show that zirconium monoxide (ZrO), present at the metal-oxide interface in pre-transition samples, is largely absent after transition [60, 80–82]. This suggests that the associated loss of oxide protectiveness may be linked to the instability of this monoxide phase.

Universality Across Ti, Zr, Ta, Nb and W

For Ti, Ta, and W, principal oxide phases are consistently reported as rutile TiO_2, Ta_2O_5, and WO_3 [17, 26, 44, 45, 83, 84], respectively. This makes transitions to porous higher-valence oxides as proposed for Nb ("Formation of Porous Oxides" Section), or transformations within the principal oxide such as the T → M transition in Zr ("Phase Transformation Within the Principal Oxide" Section), less likely as general explanations. In contrast, localized phase evolution at the metal-oxide interface ("Phase Instability at Metal-Oxide Interface" Section) may provide a possible

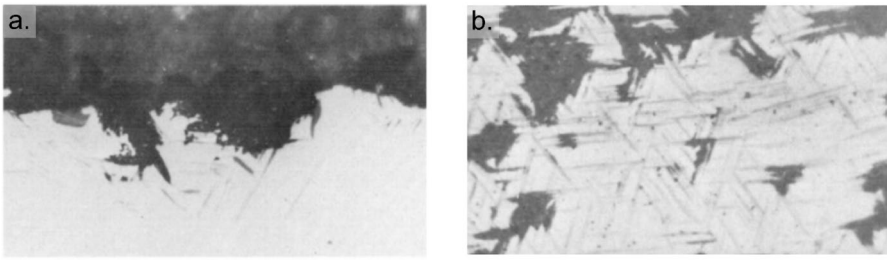

Fig. 5 Suboxide platelets associated with interfacial degradation in Nb and Ta observed in **a** the cross-section of oxidized Nb and **b** the exposed Ta surface after bulk oxide removal. Panel (a) reprinted and panel (b) adapted from [27] with permission from Elsevier

common basis for the loss of oxide protectiveness in early transition metals. This hypothesis is developed further in "Proposed Role in Oxide Degradation" Section.

Kinetic Mechanisms

Breakaway oxidation has been associated with various diffusion and reaction processes involving defects in the principal oxides that form on early transition metals. The principal oxides reported for Ti, Zr, and W, namely TiO_2, ZrO_2, and WO_3, are generally associated with n-type transport involving oxygen vacancies [5, 26, 45, 61, 62]. In Ta, the principal oxide is typically Ta_2O_5 [4, 17], whereas Nb_2O_5 or NbO_2 has been reported in Nb depending on the oxidation conditions [19, 24]. Reports on the defect structure of Ta and Nb oxides are more limited and less consistent: some studies indicate that oxygen vacancies dominate [41, 51], whereas others invoke diffusion of oxygen interstitials as the rate-controlling mechanism under specific oxidation conditions [17, 72]. Condensation of oxygen vacancies at the metal-oxide interface may form pores that degrade scale adherence [41, 85–87]. However, such pores are expected to be nanometer-scale [87], unlike the micron-scale features in Figs. 3 and 4.

In Zr alloys, vertically aligned nanopores formed via a Kirkendall mechanism within the ZrO_2 scale (Fig. 6a) have been proposed to connect with lateral pores (such as those shown in Fig. 4) to form rapid oxygen pathways [2, 37, 38, 70]. O-18 tracer profiles support the presence of such pathways in post-transition samples (Fig. 6b). However, because this Kirkendall mechanism depends on alloying-element effects, it cannot explain breakaway in early transition metals [88].

Because breakaway behaviors and periodically layered oxide morphologies (Figs. 1 and 3) are not readily described by classical oxidation models, instabilities such as Hopf-type chemical instabilities and Turing-type diffusional instabilities have been explored as possible explanations [89–91]. For instance, periodically layered oxide formation in Ti-Zr alloys is attributed to oscillatory transformation between porous, sub-stoichiometric $TiZrO_4$ to a compact, stoichiometric $TiZrO_4$, which in

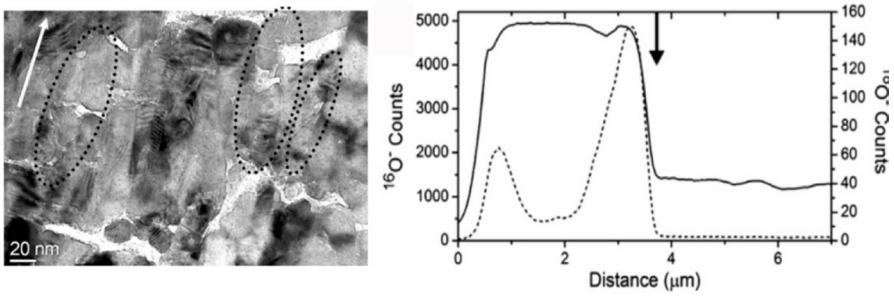

Fig. 6 **a** Regions with nanopores (circled) observed shortly after the first transition in the oxidation kinetics of a Zr alloy. The arrow indicates the direction of oxide growth. **b** Near-transition samples showing a strong spike in O-18 tracer near the metal-oxide interface (marked by the arrow) indicate the presence of a barrier-free path within the oxide. Reprinted from [80] with permission from Elsevier

turn is proposed to be driven by thermal feedback from the exothermic oxidation reaction (Fig. 7) [90]. Experimental validation of such instabilities in pure metals, however, remains limited.

Overall, experimental studies suggest plausible ways in which defects within the principal oxide may contribute to loss of oxide protectiveness, while theoretical chemical- and diffusional-instability frameworks remain largely unvalidated. None of these mechanisms appear sufficient to explain breakaway across all early transition metals in isolation. A promising direction is therefore to examine kinetic degradation processes beyond the principal oxide, including those associated with defect-rich oxide phases that form locally near the metal-oxide interface, as discussed further in "Proposed Unifying Breakaway Factors" Section.

Proposed Unifying Breakaway Factors

"Physical Mechanisms, Thermodynamic Mechanisms, Kinetic Mechanisms" Sections highlight that existing studies provide an incomplete and occasionally contradictory mechanistic understanding of breakaway. Indeed, distinct mechanisms have been proposed even within individual metals, e.g., formation of higher-valence oxides and interfacial phase transformation in Nb. A unified assessment of the available evidence instead suggests that the structure and evolution of the metal-oxide interface may provide a possible common basis for the loss of oxide protectiveness ("Universality Across Ti, Zr, Ta, Nb, and W" Section).

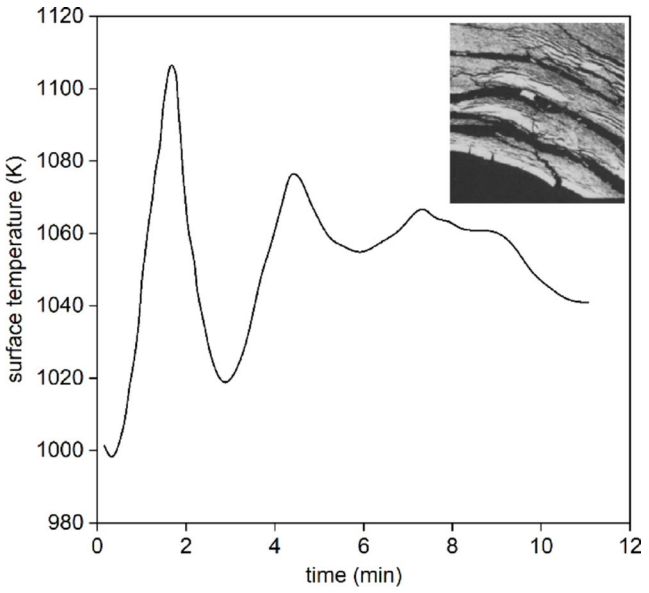

Fig. 7 Temporal oscillations in the surface temperature of Ti-Zr alloys during oxidation. Inset shows the corresponding stratified oxide scale. Data replotted and insert adapted from [90] with permission from Elsevier

Oxygen Dissolution in Metal

Across Ti, Zr, Nb, and Ta, experimental and thermodynamic evidence supports substantial oxygen dissolution into the metal lattice to form oxygen-rich solid solutions denoted here as M(O) [17, 24, 51, 60, 80, 92, 93]. Quantitative oxygen-content measurements after oxidation are relatively sparse, and the evidence for a direct link between M(O)-related instabilities and breakaway varies across metals (Table 2). While the thermodynamic solubility limit provides an approximate upper bound, the actual oxygen content reached during oxidation depends on the temperature, oxygen partial pressure, exposure time, alloy composition, and the phases present at the metal-oxide interface. Oxygen contents exceeding the thermodynamic solubility limit have also been reported, e.g., in Ta below 700 ° C, and they are typically attributed to metastable suboxides [17, 24, 80].

In Ta and Nb, oxygen oversaturation in the metal and subsequent transformation of oxygen-rich interfacial regions into platelet-like suboxides observed at the interface has been used to explain metal fragmentation and breakaway (Table 2, "Phase Instability at Metal-Oxide Interface" Section). For Ti and Zr, substantial oxygen dissolution is well established, but its direct role in breakaway remains unresolved. For W, thermodynamic oxygen solubility is extremely low, and both oxygen uptake measurements and interfacial phase characterization during oxidation remain limited.

Reported suboxides below MO composition are also included in Table 2. In some metals, such as Nb, these suboxides have been linked to breakaway. The following section examines the separate evidence for monoxide phases and their potential role in breakaway.

Monoxide Formation

Experimental evidence across Ti, Zr, Nb, and Ta indicates the formation of monoxide (MO) phase, although the strength and relevance of this evidence varies substantially across systems (Table 3). Zr alloys provide the strongest evidence, with interfacial cubic ZrO directly identified in thermally grown oxides by APT, EELS, and electron diffraction. Importantly, an interfacial ZrO layer has also been reported during oxidation of pure Zr using APT, indicating that this phase is not necessarily restricted to Zr alloys [63]. NbO has been detected by XRD at exposed metal-oxide interfaces following high-temperature oxidation. XRD analysis has also suggested TaO and TiO formation during high-temperature oxidation, although their interfacial localization remains inferred rather than directly demonstrated. For W, analogous WO formation has not been confirmed.

The association between MO evolution and kinetic transitions is strongest in Zr alloys. An interfacial ZrO layer identified at the metal-oxide interface in thermally grown oxides is generally absent after the kinetic transition ("Phase Instability at Metal-Oxide Interface" Section). This layer is typically reported to have a cubic crystal structure and a thickness of the order 10–100 nm. Detailed characterization has revealed that it consists of two sublayers, a super-stoichiometric ($ZrO_{(1+x)}$) layer and a relatively thinner sub-stoichiometric ($ZrO_{(1-x)}$) layer beneath it [60, 99].

Table 2 Thermodynamic oxygen solubility in the metal, reported local oxygen contents after oxidation, and oxygen-stabilized phases below monoxide composition in Ti, Zr, Nb, Ta, and W. Thermodynamic solubility values, oxygen contents, and temperatures are approximate

Early transition metal/alloy	Approximate maximum thermodynamic O solubility in metal phase (at% O)	Reported maximum O content in metal after oxidation (at% O)	Reported suboxides below monoxide (MO) composition	Evidence for breakaway relevance
Ti	30 at 1900 ° C [94]	12–20 at 600–700 ° C; 19–25 at 700–900 ° C; [92]	Ti_2O, Ti_6O [92, 95]	No direct link identified
Zr alloy	29 below 1200 ° C in Zr metal [80]	2–20 at 300 ° C [60] 29–30 at 360 ° C [80]	Zr_3O [60]	No direct link identified
Nb	10 at 1900 ° C [96]	1.4 at 775 ° C [97]	NbO_x, NbO_z below 600 ° C [31]	Breakaway linked to metal exfoliation associated with transformation of oxygen-saturated Nb to a suboxide [27] and oxidation of NbO_z platelets [52]
Ta	5 at 1500 ° C [98]	2.2–3 at 800–1000 ° C; 5–7 below 700 ° C; [17]	TaO_y, TaO_z/Ta_2O below 800 ° C [4, 51]	Breakaway linked to metal exfoliation associated with transformation of oxygen-saturated Ta to a suboxide [27]
W	$\sim 10^{-4} - 10^{-3}$ (reported as a few ppm, temperature not specified) [41]	Not identified	Not identified	No direct link identified

Table 3 Summary of the experimental evidence for monoxide (MO) formation and its association with breakaway behaviors in Ti, Zr, Nb, Ta, and W

Early transition metal/alloy	Experimental evidence for MO formation	Evidence for link with breakaway behaviors	Evidence hierarchy
Ti	TiO detected by XRD under high-temperature low-p_{O_2} conditions [95], XPS depth profiling of thin UHV-grown oxides [100], SAED patterns of thin oxides formed on Ti powders [101]	No direct link identified	MO detected in thermally grown oxides; interfacial localization indicated in thin oxides; breakaway link absent
Zr alloy	APT, EELS, and electron diffraction showing interfacial cubic ZrO of the order 10–100 nm thickness grown at high temperatures [47, 60, 80, 81]	ZrO generally absent post-transition [47, 80]	Direct interfacial MO evidence in thermally grown oxides; transition-associated disappearance
Nb	NbO detected by XRD after etching to expose the metal-oxide interface in samples oxidized at high temperature and sub-atmospheric oxygen pressure [31], AES/XPS on oxide formed at room-temperature, low-p_{O_2} conditions [102]	No direct link identified	Interfacial MO detected under high-temperature oxidation; breakaway link absent
Ta	TaO detected by XRD in oxides grown above 800 °C [17], AES/XPS on oxides formed at room-temperature, low-p_{O_2} conditions [102]	TaO formation inferred to coincide with formation of periodically layered oxide scale, both reported above 800 °C [4]	MO detected under high-temperature oxidation; interfacial localization inferred; link to layered oxide morphology inferred
W	No WO detected by Raman spectroscopy at ~1 µm spatial resolution [103]	No direct link identified	MO unconfirmed

UHV, ultra-high vacuum; APT, atom probe tomography; EELS, electron energy-loss spectroscopy; AES, Auger electron spectroscopy; XPS, X-ray photoelectron spectroscopy; XRD, X-ray diffraction; SAED, selected-area electron diffraction. Reported observations should not be interpreted as universal across all oxidation conditions

Evidence for Ta is more suggestive: appearance of periodically layered oxides above 800 °C coincides with TaO formation instead of TaO_Z, but direct evidence of TaO evolution at the metal-oxide interface is lacking [4]. For Ti and Nb, a direct link of the MO phase to breakaway behaviors has not yet been established. For W, MO formation has not yet been confirmed. Higher-resolution interfacial characterization is therefore needed, as Raman spectroscopy alone may be insufficient to detect thin buried interfacial layers analogous to the ZrO layers observed in Zr-based systems.

Proposed Role in Oxide Degradation

Taken together, these observations suggest that localized interfacial instabilities associated with the solid-solution M(O) and the MO phase may provide a possible unified basis for the underlying loss of oxide protectiveness, although the strength of supporting evidence varies across systems (Fig. 8).

Formation of oxygen-rich metal, M(O), beneath the oxide scale may generate volumetric strain in the metal lattice, promote near-interface embrittlement or cracking, or modify the thermodynamic stability of phases at the metal-oxide interface [27, 52, 104]. Under continued oxidation, oxygen-rich metal may transform into monoxide or other suboxides, producing additional local strains and disrupting the continuity of the protective oxide scale. In Ta and Nb, this type of process has been invoked to explain platelet-like suboxide formation, metal fragmentation, and breakaway ("Oxygen Dissolution in Metal" Section).

MO phases may provide an additional route to interfacial instability. These monoxides are typically reported to adopt a cubic rock-salt structure and to accommodate large deviations from stoichiometry through Schottky-type disorder, involving

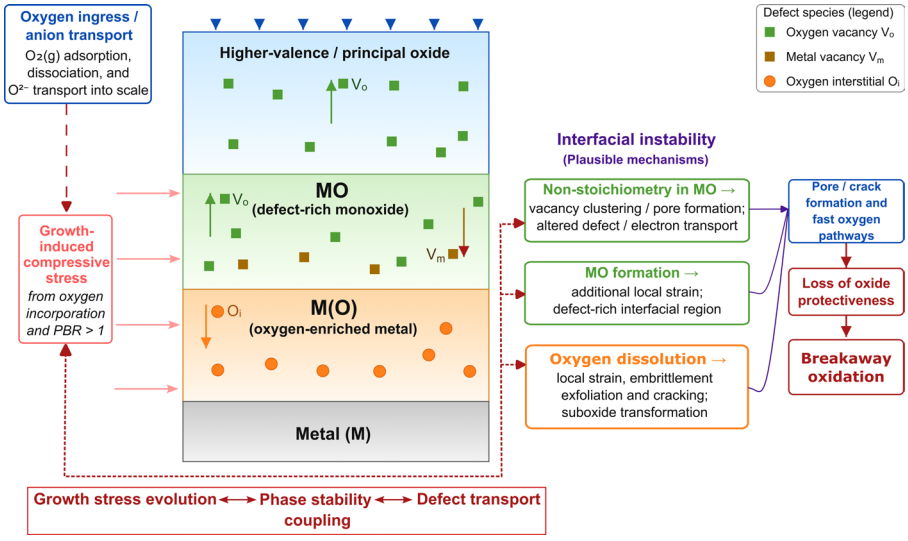

Fig. 8 Schematic representation of the unifying framework proposed for breakaway oxidation in early transition metals, involving interfacial instabilities associated with the monoxide (MO), oxygen-enriched metal (M(O)), and compressive stresses induced by oxygen uptake

vacancies in both the metal and oxygen sublattices [41, 82, 105]. Such defect structures can enable metal-like cond uctivity, influencing local transport behavior at the metal-oxide interface [41, 82]. Stoichiometric deviations in MO phases, such as those experimentally reported in Zr alloys ("Monoxide Formation" Section), may make the metal-oxide interface susceptible to local instability, potentially through vacancy clustering or pore formation.

Interfacial phase evolution and growth stresses may be mutually coupled: oxygen dissolution and M(O)/MO evolution can introduce local strains, while stress-modified phase stability and defect transport may favor defect accumulation, vacancy clustering, and localized pore or crack formation. Such interfacial instabilities may occur periodically, with each transition approximately resetting the oxidation kinetics to a new diffusion-limited growth segment and enabling a subsequent loss of oxide protectiveness. This repeated sequence may explain the formation of periodically layered oxides and repeated kinetic transitions (Fig. 3).

Although evidence of such interfacial instabilities is currently limited to Ta, Nb, and Zr ("Oxygen Dissolution in Metal, Monoxide Formation" Sections), this framework provides a testable hypothesis for early transition metals more broadly. W is an important limitation: available studies have not confirmed an interfacial MO phase, oxygen uptake measurements during oxidation remain limited, and the thermodynamic oxygen solubility in W is low (Tables 2 and 3). If W does not form a stable or metastable interfacial MO under relevant oxidation conditions, then MO-associated instability cannot be considered universal across early transition metals. Advanced characterization is needed to determine whether this reflects a true mechanistic exception or insufficient interfacial resolution. Overall, interfacial characterization in Ti, Nb, Ta, and W remains less developed than in Zr-based systems. Comparable APT, EELS, and STEM analyses are needed to determine the presence, chemical composition, crystal structure, and temporal evolution of interfacial phases before and after the acceleration in oxidation kinetics associated with breakaway.

The relevance of the proposed M(O)/MO framework to Hf, V, and Mo is expected to be metal-specific. Hf is the most plausible extension because of its chemical similarity to Ti and Zr, as well as high oxygen solubility [106]. V and Mo are less direct extensions. This is because high-temperature oxidation can be dominated by melting of vanadium pentoxide (V_2O_5) above 675 °C [39], while molybdenum trioxide (MoO_3) can volatilize above 750 °C [107]. Thus, in V and Mo, lower-temperature regimes below the onset of significant oxide melting or volatilization may provide better tests of whether M(O)/MO-associated interfacial instabilities can occur.

Oxide Growth Kinetics

Before linear breakaway: Across Ti, Zr, Nb, Ta, and W, the roughly parabolic segments observed before linear breakaway, including segments between periodic transitions (Fig. 1), are controlled by solid-state diffusion. The rate-controlling mechanism, especially in Ti, Zr, and W, is generally reported as oxygen transport via anion vacancies (n-type) [5, 26, 44, 45, 61, 62], sometimes supplemented by grain-boundary diffusion [45, 108, 109]. As discussed in Sec. 2.5.1, oxygen dissolution into the sub-

strate to form M(O) is important in Ti, Zr, Nb, and Ta [4, 5, 24, 80, 95], and its contribution to the overall weight gain is particularly significant in Ti and Zr [41, 83]. Some studies, particularly in Ta and Nb, suggest an oxygen interstitial (p-type) transport to explain the observed pressure dependence of oxidation rate under certain conditions [17, 24]. A detailed analysis is needed to determine whether this behavior reflects true p-type transport or n-type diffusion with a pressure-dependent defect population.

After linear breakaway: The linear kinetics in this regime is commonly interpreted as interface-controlled, either by the oxidation reaction at the metal-oxide interface or by oxygen incorporation at the gas-solid interface. However, as noted in "Shared Oxidation Characteristics" Section, the apparent linear behavior in early transition metals may instead arise from rapid cyclic formation and breakdown of thin barrier sub-layers, in which case the effective linear rate reflects the sub-layer thickness and regeneration time rather than a single interfacial process. While a $p_{O_2}^{0.5}$ dependence is typically associated with reaction-controlled kinetics [17, 18, 24], deviations from this behavior are either attributed to adsorption-desorption processes at the gas-solid interface [72, 110], a p-type diffusion through a thin barrier layer [72], or a decrease in the periodic sub-layer thickness with increasing oxygen partial pressure [19]. Systematic studies correlating the oxygen partial pressure with oxide morphology and kinetics are essential to identify the rate-controlling mechanisms in the post-linear-breakaway regime.

Linear Breakaway Conditions

Figure 9 shows typical trends in the time to reach linear breakaway and the corresponding weight gain. In most early transition metals, higher temperatures accelerate the onset of linear breakaway (Fig. 9a). The associated weight gain generally increases with temperature (Fig. 9b), suggesting greater total oxygen uptake and, where oxide-scale growth is the dominant contribution, formation of a thicker oxide

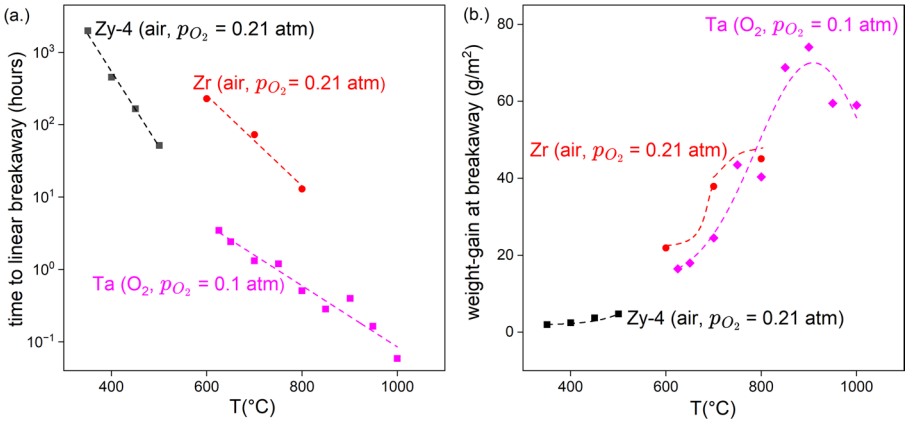

Fig. 9 **a** Time required to reach linear breakaway versus temperature. **b** Weight gain at breakaway versus temperature.

before the loss of protectiveness. This trend may arise from enhanced stress relaxation or delayed phase instabilities at elevated temperatures. Deviations from this trend are observed for Ta at higher temperatures, which may reflect partial spallation during cooling (reducing the measured weight gain) or a change in the dominant breakaway mechanism. Additional targeted studies are needed to resolve this deviation in Ta behavior.

Given the link between periodically layered oxide morphology and linear breakaway (Shared Oxidation Characteristics" Section), Fig. 10 compiles the periodic sub-layer thickness as a function of temperature. This thickness generally increases with temperature, a behavior consistent with the weight-gain trend (Fig. 9b). However, the limited data available for Ti deviates from this behavior. One possible explanation is that elevated temperatures expand the Ti-O composition range over which γ-TiO phase is stable, a phase known to tolerate large deviations from stoichiometry [105, 111]. If monoxides influence the breakaway behavior as suggested in "Proposed Unifying Breakaway Factors" Section, it can explain the distinct response observed for Ti.

Note that the data in Figs. 9 and 10 are compiled from stud ies with different atmospheres, oxygen partial pressures, and material purity or alloy composition. In addition, weight gain at breakaway does not correspond uniquely to oxide thickness because it may include contributions from oxygen dissolved in the metal and, in some cases, local oxide spallation. They are therefore interpreted only as qualitative trends. Across early transition metals, trends in time to linear breakaway, mass gain at linear breakaway, and periodic sub-layer thickness are broadly consistent. Ti emerges as a

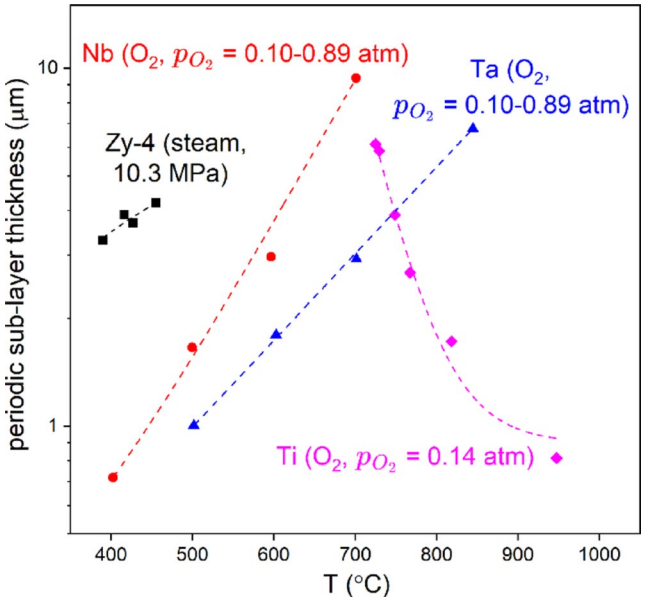

Fig. 10 Periodic sub-layer thickness versus temperature. Source-study conditions are: Ti in O_2 ($p_{O_2} = 0.14$ atm) [57], Zircaloy-4 in 10.3 MPa steam [29], and Ta and Nb in O_2 ($p_{O_2} = 0.10 - 0.89$ atm) [50]. Reported p_{O_2} values are nominal.

notable outlier, further highlighting the need to assess the role of the MO phase to establish a unified understanding.

Comparative Assessment of Oxidation Behavior and Breakaway Evidence

"Mechanistic Review of Breakaway and Oxide Growth Kinetics" Sections show that Ti, Zr, Nb, Ta, and W exhibit shared oxidation characteristics but also important differences in their breakaway behavior, oxygen dissolution, transport characteristics, and the strength of evidence for interfacial phase structure and its evolution. Table 4 synthesizes these observations across the five primary systems. The comparison distinguishes directly observed phenomena from inferred associations and unconfirmed cases, providing an evidence-based basis for evaluating the proposed interfacial-instability framework and identifying priorities for future experimental and modeling studies.

Breakaway Models

The transport processes governing the roughly parabolic segments observed before linear breakaway are reasonably described by diffusion-based models that incorporate effects such as evolving grain structure, oxygen dissolution into the substrate, multiphase oxide formation, and space-charge phenomena [5, 92, 108, 114]. However, mechanistic models addressing the loss of oxide protectiveness that drives breakaway remain limited. These models are summarized in Table 5 and are classified based on the physical, thermodynamic, or kinetic mechanisms they invoke ("Mechanistic Review of Breakaway" Section, Fig. 2).

The modeling efforts synthesized in Table 5 provide useful insights into potential causes of breakaway. However, experiments rarely provide the data required to identify the underlying mechanism unambiguously. As a result, multiple distinct mechanisms have been used to explain breakaway even within a single system such as Zr alloys. This has led to a fragmented and contradictory mechanistic picture, consistent with trends in the experimental literature ("Proposed Unifying Breakaway Factors" Section). Recent theoretical work demonstrates that a diffusional instability in a moving-boundary reaction-diffusion system (e.g., a growing oxide with a moving metal-oxide interface) can generate spatiotemporal periodic behaviors similar to those observed in early transition metals (Fig. 11) [91]. This highlights its potential as a possible unifying framework for modeling breakaway. However, the approach remains largely abstract and has not yet been linked to specific defect species, phase evolution, or stress development in real materials.

Overall, none of the existing models can definitively explain breakaway in early transition metals. A key limitation is that they do not capture the evolving metal-oxide interface or the coupling of stresses, phase evolution, and defect transport that may give rise to interfacial instabilities ("Proposed Role in Oxide Degradation" Section). Instead, they either focus on isolated phenomena within the principal oxide,

Table 4 Cross-metal comparison of typical oxidation behavior and evidence relevant to the proposed framework in Ti, Zr, Nb, Ta, and W. Thermodynamic solubility and oxygen uptake values are approximate and condition-dependent; detailed data and evidence hierarchy are provided in Tables 2 and 3. Reported behaviors and observations should not be interpreted as universal across all oxidation conditions

Early transition metal/alloy	Principal oxide scale and diffusion mechanism	Oxygen dissolution in metal	Typical breakaway behavior	Representative periodicity/layering observations	Evidence relevant to the proposed framework
Ti	Rutile TiO_2; generally associated with n-type oxygen transport involving oxygen vacancies	High; thermodynamic solubility up to 30 at% O. Reported oxygen contents after oxidation: 12-25 at%	Weak periodic transients followed by linear breakaway	Layered oxides reported; formation of new sublayers is associated with weak periodic fluctuations, and layering can persist after linear breakaway	MO detected in thermally grown oxides, but interfacial localization remains inferred; a direct link between interfacial MO, M(O), and breakaway has not been established
Zr alloy/pure Zr	ZrO_2; generally associated with n-type oxygen transport involving oxygen vacancies	High; thermodynamic solubility up to 29 at% O. Reported oxygen contents after oxidation: 2-30 at% in Zr alloys	Zr alloys: periodic kinetic transitions followed by linear breakaway; direct linear breakaway in pure Zr	In Zr alloys, periodic layering directly correlates with kinetic transitions and can persist after linear breakaway; layering reported in pure Zr	Direct interfacial MO evidence in thermally grown oxides in both Zr alloys and pure Zr; kinetic transition-associated disappearance in Zr alloys
Nb	Nb_2O_5 or NbO_2 depending on oxidation conditions; dominant diffusion mechanism and defect species remains uncertain	Moderate; thermodynamic solubility up to 10 at% O. Reported oxygen content: 1.4 at%	Direct linear breakaway	Layered oxides reported in linear kinetics regime	M(O) regions and suboxide platelets linked to metal fragmentation during breakaway. MO detected at an exposed metal-oxide interface, but its role in breakaway is unestablished
Ta	Ta_2O_5; dominant diffusion mechanism and defect species remains uncertain	Moderate; thermodynamic solubility up to 5 at% O. Reported oxygen contents: 2.2-7 at%	Direct linear breakaway	Layered oxides reported in linear kinetics regime	Transformation of M(O) to suboxide phases linked to metal exfoliation and breakaway; reported MO formation occurs in the same temperature range as layered oxide formation, but interfacial localization remains inferred
W	WO_3; generally associated with n-type oxygen transport involving oxygen vacancies	Low; on the order of few ppm	Irregular weak transients followed by linear breakaway	Layered oxides are reported before and after linear breakaway	Significant oxygen uptake in the metal and an analogous interfacial MO phase remain unconfirmed

Table 5 Models and theoretical frameworks proposed for breakaway in oxidation kinetics

	Systems	Mechanisms	Prediction	Limitations	References
Porosity model	Ti	Kinetic (diffusion through a porous oxide layer)	Parabolic kinetics at short times; Linear kinetics at long times	Assumes the presence and evolution of porosity; lacks experimental validation	[26]
Lateral cracking model	Zr alloys	Physical (cracking parallel to the metal-oxide interface driven by interface undulations	Tensile stresses that explain cracking	Does not explain how isolated lateral cracks cause loss of protectiveness	[35]
Radial cracking model	Zr alloys	Physical (through-thickness oxide cracking on a curved substrate	Critical oxide thickness for stresses to become tensile and drive cracking	Contradicted by flat-specimen studies showing no such cracks	[42, 72, 115]
Phase transformation model	Zr alloys	Thermodynamic (stress-driven tetragonal → monoclinic ZrO_2 transformation	Critical oxide thickness at which transformation becomes favorable	Limited validation and not applicable to other early transition metals	[113]
Hopf bifurcation model	Generic	Kinetic (nonlinear chemical instability)	Purely oscillatory oxidation kinetics	Does not account for diffusion and lacks validation in real systems	[116]
Diffusional-instability model	Generic	Kinetic (oxidation as a reaction-diffusion system with a Turing instability)	Sub-linear kinetic growth segments separated by periodic kinetic transitions	Still theoretical and lacks link to real systems	[91]

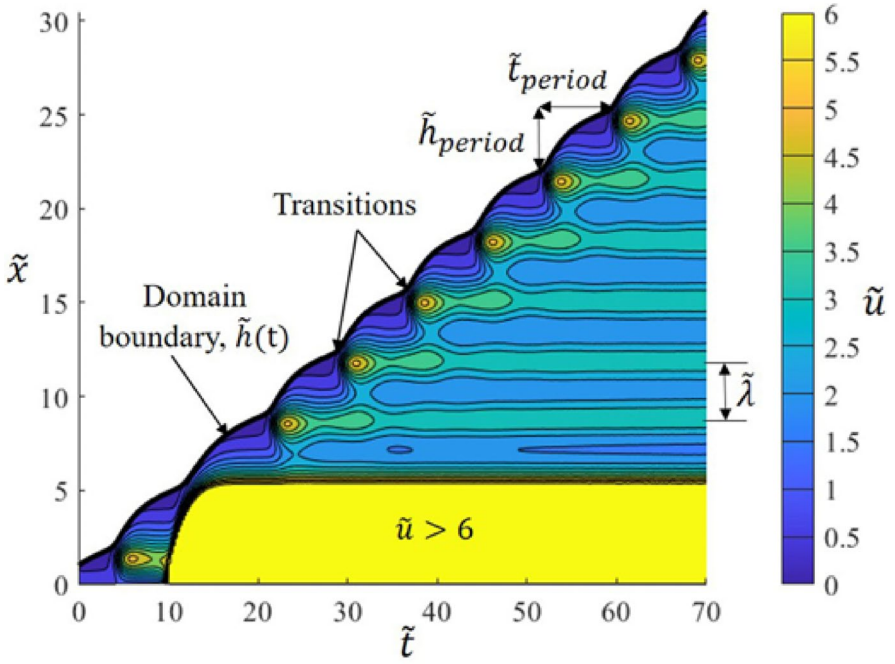

Fig. 11 Theoretical study based on a Turing diffusional instability reproducing spatiotemporal periodic behavior observed experimentally (Figs. 1, 3). Contours represent the concentration of a chemical species (u) that influences the oxidation rate. Reprinted figure with permission from I. [91], Fig. 1(a). Copyright © 2020 by the American Physical Society; https://doi.org/10.1103/physreve.102.012802

such as cracking or phase transformations, or lack a connection with real materials, such as those based on kinetic instabilities.

Future modeling efforts must move beyond single-mechanism descriptions and instead incorporate the coupled evolution of interfacial phase structure (M(O) and MO), defect transport through multiple phases, and growth stress development. Capturing this interplay at the metal-oxide interface is essential for developing physically grounded models of breakaway that are applicable across early transition metals.

Strategies to Enhance the Oxidation Resistance

Various alloying and processing strategies have been proposed to reduce oxidation rates in early transition metals and suppress breakaway. These approaches commonly aim to limit the oxygen ingress by stabilizing dense protective oxide or nitride layers, improving oxide-scale adhesion, reducing fast transport pathways, or introducing residual surface stresses. Consistent with the factors identified in "Proposed Role in Oxide Degradation" Section, many reported strategies, particularly in Ti, Zr, Nb, and Ta, mitigate oxygen dissolution in the metal either directly, by reducing the solubility limit or oxygen diffusivity, or indirectly, by limiting the oxygen ingress to the metal-oxide interface. The individual strategies are outlined below.

Alloying Strategies

Alloying strategies across Ti, Zr, Nb, Ta, and W achieve an improved oxidation resistance via three main routes:

1. Reduction of oxygen solubility in the metal substrate (e.g., Al addition in Ti).
2. Stabilization of dense, protective oxide scales (e.g., Al, Si, Cr additions).
3. Improved adhesion between the oxide and the substrate (e.g., Y addition).

The key alloying additions and the mechanism through which they enhance the oxidation resistance are summarized in Table 6. It is important to note that the effect of individual alloying elements is strongly influenced by its weight fraction, other alloying elements, and by processing history [32].

Processing and Microstructure Tailoring Strategies

Processing and microstructural tailoring techniques proposed to improve the oxidation resistance of Ti, Zr, Nb, Ta, and W are summarized in Table 7, and they can be broadly classified into three categories:

Table 6 Summary of alloying effects that improve the oxidation resistance

Early transition metal/alloy	Alloying element	Mechanism of enhanced oxidation resistance
Ti	Nb, Ta	Promote protective interfacial Ti_2N scale which limits oxygen dissolution in metal [117, 118]
	W	Also favors protective interfacial Ti_2N [117, 119]
	Al	Decreases O diffusivity in Ti, thereby reducing oxygen dissolution [119, 120]
	Si	Promotes protective interfacial Ti_2N and Ti_5Si_3 scales; may also reduce oxygen solubility limit [120–122]
Zr	Cr, Fe, Ni	Promote more uniform oxidation and delays premature spalling, improving scale adhesion [71]
Nb	Ti, Hf, Zr, V	Decrease oxygen diffusivity in Nb; favors compact TT-Nb_2O_5 phase [123]
Nb (from Nb-Si-based studies)	Cr	Reduces oxygen diffusivity in the alloy; forms protective $CrNbO_4$ scale [124]
	Al	Reduces oxygen diffusivity in the alloy; forms protective Al_2O_3 scale [124]
	Si	Forms protective SiO_2 scale, hindering oxygen diffusion [124]
	Sn	Sn-based phases reduce oxygen diffusivity and oxygen penetration into metal [125]
Ta (from Ta-W studies)	Al	Protective Al_2O_3 scale [126]
W	Si	Protective SiO_2 scale [127]
	Cr	Protective Cr_2WO_6 or Cr_2O_3 scale [127, 128]
	Y	Improves adhesion between the oxide film and the substrate [127]
	Al	Protective Al_2O_3 scale [128]
	Ti	Protective TiO_2 scale [128]

Table 7 Summary of processing and microstructural tailoring strategies to improve the oxidation resistance

Early transition metal/alloy	Processing/microstructural tailoring	Mechanism of enhanced oxidation resistance
Ti (Pure metal & Ti-6Al-4 V)	Nitriding	Protective Ti_2N layer formation limits oxygen dissolution into the metal/alloy [84]
Ti	Laser and shot peening	Promotes the continuity of protective Ti_2N scale, reducing oxygen dissolution [129]
Ti (Pure metal & Ti–0.6Y_2O_3)	Powder metallurgy	Suppresses periodic oxide layering, suggesting reduced cyclic loss of oxide protectiveness [118]
Ti-Al-Si alloy	Mechanical alloying	Performs better than reactive sintering, likely due to a lower porosity that limits fast oxygen ingress [130]
Zr	Shot peening	Residual compressive stress slows oxygen diffusion in the metal [131]
Nb	Nitriding	Protective Nb_2N and NbN layer which oxidizes slower than Nb, together reducing overall growth rate [132, 133]
Ta	Single crystal	Prevents grain boundary diffusion compared to polycrystalline Ta [51]
	Texture control	Single crystals with {100} faces oxidize slowest [49]
W	Texture control	Least oxidation at {111} surfaces for T = 447–597 ° C [134] and at (110) surface for T > 1800 ° C [135]

1. Modification of near-surface chemistry, such as nitriding, which promotes the formation of protective layers.
2. Control of microstructural transport pathways by tailoring grain size and texture.
3. Introduction of residual stresses, for example through shot-peening, which may slow down oxygen diffusion into the metal.

The effectiveness of these approaches depends strongly on the operating temperature and alloying chemistry.

Relevance to Refractory High-Entropy Alloys

Early transition metals are often encountered constituents in refractory high-entropy alloys (RHEAs), a relatively new class of materials considered as promising candidates for structural applications at ultra-high temperatures [9, 136–139]. However, the oxidation behavior of RHEA has raised concern due to widespread pest oxidation, volatilization, fast oxidation rates, scale spallation and breakaway oxidation kinetics [140]. In general, only few RHEA (systems) form protective oxide scales such as Al_2O_3 [141], $CrTaO_4$ [142] or $CrTaTiO_6$ [143] that grow parabolically as a result of the solid-state diffusion of cations and/or anions.

Unfortunately, most early transition metals either prevent the formation of protective scales or causes their fast degradation. In addition to the high oxidation rates discussed above, Table 8 summarizes further detrimental effect of these elements if added to RHEA in notable concentrations, typically between 10 and 30 at%. The

Table 8 Summary of the influence of early transition elements on the oxidation of RHEA

Element	Positive effects on RHEA oxidation	Negative effects on RHEA oxidation
Ti	Supports the formation of protective complex oxides $CrTaO_4$ and $(Cr, Ta, Ti)O_6$ [143]	High oxygen solubility in α-Ti [144]
Zr		High oxygen solubility in α-Zr [145] Supports pesting by increasing the volume of the oxides [146] Forms fast growing ZrO_2
Hf		High oxygen solubility [106] Supports pesting by increasing the volume of oxides [146]
V		Oxide melts above 675 °C [39] High PBR [147]
Nb		High oxygen solubility [27] High PBR [148] Forms polymorphic oxides [149]
Ta	Increases the temperature required to form Nb_2O_5 [12] Forms protective oxides $CrTaO_4$ and $(Cr, Ta, Ti)O_6$ [143]	High oxygen solubility [150] High PBR [147]
Mo		Oxide volatilizes at 750 °C [151]
W		Oxide evaporates above 1000 °C High PBR [152]

recently performed review on high temperature oxidation behavior of RHEA revealed that Zr- and V-containing alloys demonstrate the poorest oxidation performance [13]. Even high amounts of protective oxide forming elements such as Cr and Al cannot compensate the negative impact of early transition metals mentioned above [140].

Table 8 shows that dominant negative contributors are the dissolution of oxygen into the metal lattice to form the solid solution M(O) and a high PBR that leads to large compressive growth stresses in the oxide. For example, TiZrNbHfTa has been reported to undergo alloy fragmentation attributed to extensive oxygen dissolution [13]. NbMoCrTiAl exhibits layered oxide morphologies, which have been proposed to result from repetitive alloy exfoliation associated with oxygen uptake [13]. Because oxygen dissolution, layered oxide formation, and growth stresses are also associated with breakaway oxidation of pure early transition metals ("Mechanistic Review of Breakaway" Section), these shared behaviors suggest that interfacial factors analogous to those identified in "Proposed Unifying Breakaway Factors" Section may contribute to degradation in certain RHEAs.

The proposed breakaway framework ("Proposed role in Oxide Degradation" Section) may therefore provide useful design criteria for oxidation-resistant RHEAs. First, alloy compositions should limit oxygen dissolution into the alloy, because it can embrittle the alloy, promote local phase transformations, and contribute to metal exfoliation. Alloying and processing strategies discussed in "Strategies to Enhance the Oxidation Resistance" Section that mitigate oxygen dissolution may provide pathways to achieve this. Second, alloy chemistry should avoid interfacial phase structures that favor defect-rich or highly nonstoichiometric suboxides at the advanc-

ing oxide front. Third, alloy chemistry should favor interfacial oxides with low crystallographic mismatch [153]. It should also favor oxide scales with low growth strain and limited PBR mismatch to mitigate the large compressive stresses that can drive cracking. Together, these criteria emphasize interfacial stability as a central design strategy for oxidation-resistant RHEAs.

Conclusions and Outlook

Despite decades of experimental and theoretical studies on Ti, Zr, Nb, Ta, and W, no single physical, thermodynamic, or kinetic mechanism has achieved consensus in explaining breakaway behaviors, even within individual material systems. This review therefore distinguishes between well-established common features, mechanistic links that are strongly supported in specific systems, and open hypotheses requiring further validation.

Several common oxidation features are well established across the early transition metals considered here. These include inward oxygen transport through the oxide scale, large Pilling-Bedworth ratios that generate compressive growth stresses, multiphase oxide formation, and the frequent observation of periodically layered oxide morphologies. Strongly supported mechanistic links are primarily system-specific. In Zr alloys, periodic kinetic transitions are closely associated with layered oxide formation and changes in interfacial ZrO morphology. In Nb and Ta, oxygen-rich metal regions and suboxide platelets have been linked to the loss of oxide protectiveness through metal fragmentation or exfoliation. Growth stresses are clearly relevant to oxide-scale integrity, but stress-relief cracking alone does not appear sufficient to explain breakaway. Similarly, defect-mediated mechanisms, including oxygen-vacancy condensation, Kirkendall porosity, and oscillatory instabilities, remain limited in their demonstrated generality.

The cross-metal evidence suggests that localized interfacial instabilities provide a plausible hypothesis for interpreting diverse breakaway behaviors. In this framework, oxygen enrichment of the metal to form M(O), evolution of a defect-rich monoxide (MO), and growth-induced stresses may interact to disrupt oxide-scale continuity and promote local pore formation, cracking, or fast oxygen pathways. This hypothesis remains to be fully validated. W represents an important limitation because significant oxygen uptake in the metal and an analogous interfacial monoxide phase have not been confirmed.

Future experimental efforts should therefore prioritize high-resolution, and where feasible, in-situ characterization of the evolving metal-oxide interface. Comparable APT, STEM-EELS, synchrotron-based diffraction or imaging, environmental TEM, and stress measurements across Ti, Nb, Ta, and W are needed to match the level of evidence available for Zr-based systems. Modeling efforts should move beyond single-mechanism descriptions and incorporate coupled electro-chemo-thermo-mechanical evolution of interfacial phase structure, defect transport, and growth stresses. Together, these efforts may also identify interfacial stability factors relevant to improving the oxidation resistance of refractory high-entropy alloys, where early transition metals are common constituents.

Acknowledgements The authors would like to express their sincere gratitude to Professor Michael Thouless for his critical insights on oxidation behaviors. Thanks to Sreenivas Raguraman for initial discussions on the topic.

Author Contributions I.G. - Conceptualization, Investigation, Writing—Original Draft, Writing—Review & Editing; S.T. - Investigation, Writing—Original Draft; B.R.G. - Investigation, Writing—Original Draft, Writing—Review & Editing.

Data Availability No new data were generated in this study. All data used are derived from previously published literature and are appropriately cited.

Declarations

Conflict of interest On behalf of all authors, the corresponding author states that there is no conflict of interest.

References

1. Boyer RR. Titanium for aerospace: Rationale and applications. *Adv. Perform. Mater.* 1995;2:349–368.
2. Motta AT, Couet A, Comstock RJ. Corrosion of Zirconium Alloys Used for Nuclear Fuel Cladding. *Annu. Rev. Mater. Res.* 2015;45:311–343.
3. Peters AB, Zhang D, Chen S, et al. Materials design for hypersonics. *Nat. Commun.* 2024;15:3328.
4. Angelici Avincola V, Janek M, Stegmaier U, Steinbrück M, Seifert HJ. Tantalum Oxidation in Steam Atmosphere. *Oxid. Met.* 2016;85:459–487.
5. Huang S, Kerr R, Murphy S, Gilbert MR, Marian J. Multilayer interface tracking model of pure tungsten oxidation. *Model. Simul. Mater. Sci. Eng.* 2022;30:085015.
6. Alkhamees A, Liu Y-L, Zhou H-B, Jin S, Zhang Y, Lu G-H. First-principles investigation on dissolution and diffusion of oxygen in tungsten. *J. Nucl. Mater.* 2009;393:508–512.
7. Senkov ON, Miracle DB, Chaput KJ, Couzinie J-P. Development and exploration of refractory high entropy alloys—A review. *J. Mater. Res.* 2018;33:3092–3128.
8. Senkov ON, Gorsse S, Miracle DB. High temperature strength of refractory complex concentrated alloys. *Acta Mater.* 2019;175:394–405.
9. Xiong W, Guo AXY, Zhan S, Liu C-T, Cao SC. Refractory high-entropy alloys: A focused review of preparation methods and properties. *J. Mater. Sci. Technol.* 2023;142:196–215.
10. Butler TM, Senkov ON, Daboiku TI, et al. Oxidation behaviors of CrNb, CrNbTi, and CrNbTaTi concentrated refractory alloys. *Intermetallics*. 2022;140:107374.
11. Lo K-C, Murakami H, Glatzel U, Yeh J-W, Gorsse S, Yeh A-C. Elemental effects on the oxidation of refractory compositionally complex alloys. *Int. J. Refract. Met. Hard Mater.* 2022;108:105918.
12. Butler TM, Chaput KJ. Native oxidation resistance of Al20Nb30Ta10Ti30Zr10 refractory complex concentrated alloy (RCCA). *J. Alloys Compd.* 2019;787:606–617.
13. Gorr B, Schellert S, Müller F, Christ H-J, Kauffmann A, Heilmaier M. Current Status of Research on the Oxidation Behavior of Refractory High Entropy Alloys. *Adv. Eng. Mater.* 2021;23:2001047.
14. Philips NR, Carl M, Cunningham NJ. New Opportunities in Refractory Alloys. *Metall. Mater. Trans. A*. 2020;51:3299–3310.
15. Liu CM, Wang HM, Zhang SQ, Tang HB, Zhang AL. Microstructure and oxidation behavior of new refractory high entropy alloys. *J. Alloys Compd.* 2014;583:162–169.

16. Müller F, Gorr B, Christ H-J, Chen H, Kauffmann A, Heilmaier M. Effect of Y Additions on the Oxidation Behaviour of Novel Refractory High-Entropy Alloy NbMoCrTiAl at 1000°C in Air. *Oxid. Met.* 2020;94:147–163.
17. Kofstad P. The Oxidation Behavior of Tantalum at 700°–1000°C. *J. Electrochem. Soc.* 1963;110:491.
18. Nagy D, Humphry-Baker SA. An oxidation mechanism map for tungsten. *Scr. Mater.* 2022;209:114373.
19. Sheasby JS. The Oxidation of Niobium in the Temperature Range 450°–720°C. *J. Electrochem. Soc.* 1968;115:695.
20. Gomes JEL, Huntz AM. Correlation between the oxidation mechanism of titanium under a pure oxygen atmosphere, morphology of the oxide scale, and diffusional phenomena. *Oxid. Met.* 1980;14:249–261.
21. Cifuentes SC, Monge MA, Pérez P. On the oxidation mechanism of pure tungsten in the temperature range 600–800°C. *Corros. Sci.* 2012;57:114–121.
22. Pérez P, Monge MA, Muñoz Á, Adeva P. Influence of 1 and 5 wt% TiC additions on the oxidation behaviour of pure tungsten. *Nucl. Mater. Energy*. 2020;24:100780.
23. Xu J-Y, Shi Z-Z, Zhang Z-B, Huang H-G, Liu X-F. Significant enhancement of high temperature oxidation resistance of pure titanium via minor addition of Nb and Si. *Corros. Sci.* 2020;166:108430.
24. Kofstad P, Espevik S. Low-Pressure Oxidation of Niobium at 1200°–1700°C. *J. Electrochem. Soc.* 1965;112:153.
25. Stringer J. The Effect of Nitrogen on the Oxidation of Tantalum at High Temperatures. *J. Electrochem. Soc.* 1965;112:1083.
26. Stringer J. The oxidation of titanium in oxygen at high temperatures. *Acta Metall.* 1960;8:758–766.
27. McKee I, Wallwork GR. The oxidation of tantalum and niobium in the temperature range 400 °–600°C. *J. Less-Common Met.* 1973;30:249–258.
28. Cox B. Processes occurring during the breakdown of oxide films on zirconium alloys. *J. Nucl. Mater.* 1969;29:50–66.
29. Liao J, Cheng Z, Zhang W, et al. Temperature sensitivity and transition kinetics of uniform corrosion of zirconium alloys in superheated steam. *Heliyon*. 2024;10:e33266.
30. Kofstad P, Hauffe K, Kjöllesdal H, Siekevitz P, Ernster L, Diczfalusy E. Investigation on the Oxidation Mechanism of Titanium. *Acta Chem. Scand.* 1958;12:239–266.
31. Sheasby JS, Wallwork GR, Smeltzer WW. The Parabolic Oxidation Kinetics of Niobium. *J. Electrochem. Soc.* 1966;113:1255.
32. Stoll U, Slavinskaya N. Corrosion behavior of zirconium alloys in the aqueous environment. Phenomenological aspects. Overview. *J. Nucl. Sci. Technol.* 2023;60:573–602.
33. Tran M-T, Boinet M, Galerie A, Wouters Y. Detection of breakaway oxidation with Acoustic Emission during titanium oxide scale growth. *Corros. Sci.* 2010;52:2365–2371.
34. Bryner JS. The cyclic nature of corrosion of zircaloy-4 in 633 K water. *J. Nucl. Mater.* 1979;82:84–101.
35. Vermaak N, Parry G, Estevez R, Bréchet Y. New insight into crack formation during corrosion of zirconium-based metal-oxide systems. *Acta Mater.* 2013;61:4374–4383.
36. Godlewski J. How the Tetragonal Zirconia is Stabilized in the Oxide Scale that is Formed on a Zirconium Alloy Corroded at 400°C in Steam. In: Garde A, Bradley E, eds. *Zirconium in the Nuclear Industry: Tenth International Symposium*. ASTM International; 1994:STP1245-EB .
37. Liao J, Zhang J, Zhang W, et al. Critical behavior of interfacial t-ZrO2 and other oxide features of zirconium alloy reaching critical transition condition. *J. Nucl. Mater.* 2021;543:152474.
38. Gong W, Zhang H, Wu C, Tian H, Wang X. The role of alloying elements in the initiation of nanoscale porosity in oxide films formed on zirconium alloys. *Corros. Sci.* 2013;77:391–396.
39. Tiets TE, Wilson JW. *Behavior and properties of refractory metals*. Stanford University Press; 1965.
40. Gulbransen EA, Andrew KF, Brassart FA. Oxidation of Molybdenum 550° to 1700°C. *J. Electrochem. Soc.* 1963;110:952.
41. Smeltzer WW, Young DJ. Oxidation properties of transition metals. *Prog. Solid State Chem.* 1975;10:17–54.
42. Gupta I, Barber JR, Thouless MD, Lu W. Mechanistic model for stresses in the oxide layer formed on zirconium alloys. *J. Therm. Stress.* 2019;42:1071–1082.
43. Körkel AFK, Jellesen MS, Foss M, Ceccato M, Somers MAJ, Christiansen TL. Thermochemical oxidation of commercially pure titanium; controlled formation of robust white titanium oxide layers for biomedical applications. *Surf. Coat. Technol.* 2023;467:129716.
44. Gulbransen EA, Andrew KF. Kinetics of the Oxidation of Pure Tungsten from 500° to 1300°C. *J. Electrochem. Soc.* 1960;107:619.

45. Mehrotra S, Kalyan D, Makineni SK, Santra S. Oxide growth characteristics, kinetics and mechanism of rutile formation on pure titanium. *Vacuum*. 2024;219:112682.
46. Brown Z, Brooks N, Family R, Weaver M, Davami K. The effects of laser peening on the oxidation behavior of pure titanium at 750°C. *Surf. Coat. Technol.* 2024;492:131204.
47. Preuss M, Frankel P, Lozano-Perez S, et al. Studies Regarding Corrosion Mechanisms in Zirconium Alloys. *J. ASTM Int.* 2011;8:1–23.
48. Yilmazbayhan A, Breval E, Motta AT, Comstock RJ. Transmission electron microscopy examination of oxide layers formed on Zr alloys. *J. Nucl. Mater.* 2006;349:265–281.
49. Stringer J. The high-temperature oxidation of tantalum single crystals. *J. Less-Common Met.* 1967;12:301–317.
50. Bertrand G. Pattern Formation During Dry Corrosion of Metals and Alloys. In: Walgraef D, ed. *Patterns, Defects and Microstructures in Nonequilibrium Systems*. Dordrecht: Springer Netherlands; 1987:168–186.
51. Voitovich VB, Lavrenko VA, Adejev VM, Golovko EI. High-temperature oxidation of tantalum of different purity. *Oxid. Met.* 1995;43:509–526.
52. Stringer J. The oxidation of niobium single crystals. *Acta Metall.* 1969;17:1227–1246.
53. Bouineau V, Bénier G, Pêcheur D, Thomazet J, Ambard A, Blat M. Analysis of the Waterside Corrosion Kinetics of Zircaloy-4 Fuel Cladding in French PWRs. *Nucl. Technol.* 2010;170:444–459.
54. Yang F, Zhao X, Xiao P. In Situ Measurement of Stresses and Phase Compositions of the Zirconia Scale During Oxidation of Zirconium by Raman Spectroscopy. *Oxid. Met.* 2014;81:331–343.
55. Fettré D, Favergeon J, Bouvier S. Detection of Breakaway for a High-Temperature Oxidation of Pure Zirconium Using Acoustic Emission Correlated to Thermogravimetry. *Oxid. Met.* 2017;87:367–379.
56. Dali Y, Tupin M, Bossis P, Pijolat M, Wouters Y, Jomard F. Corrosion kinetics under high pressure of steam of pure zirconium and zirconium alloys followed by in situ thermogravimetry. *J. Nucl. Mater.* 2012;426:148–159.
57. Bertrand G, Jarraya K, Chaix JM. Morphology of oxide scales formed on titanium. *Oxid. Met.* 1984;21:1–19.
58. Gomes JEL, Huntz AM. Comparison of the kinetics and morphologic properties of titanium, Ti-1.5Ni and Ti-2.5Cu during oxidation in pure oxygen between 600 and 820°C. *Oxid. Met.* 1980;14:471.
59. Pérez P. On the influence of water vapour on the oxidation behaviour of pure Ti. *Corros. Sci.* 2007;49:1172–1185.
60. Kautz EJ, Gwalani B, Lambeets SVM, et al. Rapid assessment of structural and compositional changes during early stages of zirconium alloy oxidation. *Npj Mater. Degrad.* 2020;4:29.
61. Porte HA, Schnizlein JG, Vogel RC, Fischer DF. Oxidation of Zirconium and Zirconium Alloys. *J. Electrochem. Soc.* 1960;107:506.
62. Dawson JK, Long G, Seddon WE, White JF. The kinetics and mechanism of the oxidation of zircaloy-2 at 350–500°C. *J. Nucl. Mater.* 1968;25:179–200.
63. Hudson D, Cerezo A, Smith GDW. Zirconium oxidation on the atomic scale. *Ultramicroscopy*. 2009;109:667–671.
64. Hutchinson B, Hallstadius L. Oxidation of Zircaloy-2 studied using a wedge-shaped specimen. *J. Nucl. Mater.* 2013;432:437–443.
65. Beie H, Mitwalsky A, Garzarolli F, Ruhmann H, Sell H. Examinations of the Corrosion Mechanism of Zirconium Alloys. In: Garde A, Bradley E, eds. *Zirconium in the Nuclear Industry: Tenth International Symposium*. ASTM International; 1994:STP1245-EB .
66. Ni N, Lozano-Perez S, Sykes JM, Smith GDW, Grovenor CRM. Focussed ion beam sectioning for the 3D characterisation of cracking in oxide scales formed on commercial ZIRLO™ alloys during corrosion in high temperature pressurised water. *Corros. Sci.* 2011;53:4073–4083.
67. Bossis P, Lelièvre G, Iltis X, Lefebvre F, Barberis P. Multi-Scale Characterization of the Metal-Oxide Interface of Zirconium Alloys. In: *Zirconium in the Nuclear Industry: Twelfth International Symposium*. ASTM International; 2000; 918–945.
68. Parise M, Sicardy O, Cailletaud G. Modelling of the mechanical behavior of the metal–oxide system during Zr alloy oxidation. *J. Nucl. Mater.* 1998;256:35–46.
69. Polatidis E, Frankel P, Wei J, et al. Residual stresses and tetragonal phase fraction characterisation of corrosion tested Zircaloy-4 using energy dispersive synchrotron X-ray diffraction. *J. Nucl. Mater.* 2013;432:102–112.
70. Ni N, Lozano-Perez S, Sykes J, and Grovenor C. Multi-scale characterisation of oxide on zirconium alloys. *Mater. High Temp.* 2012;29:166–170.

71. Cox B. Some thoughts on the mechanisms of in-reactor corrosion of zirconium alloys. *J. Nucl. Mater.* 2005;336:331–368.
72. Nakamura J, Hashimoto M, Otomo T, Kawasaki S. Effects of oxygen partial pressure on oxidation of Zircaloy. *J. Nucl. Mater.* 1993;200:256–264.
73. Sundell G, Thuvander M, Andrén H-O. Tin clustering and precipitation in the oxide during autoclave corrosion of Zircaloy-2. *J. Nucl. Mater.* 2015;456:409–414.
74. Yilmazbayhan A, Motta AT, Comstock RJ, Sabol GP, Lai B, Cai Z. Structure of zirconium alloy oxides formed in pure water studied with synchrotron radiation and optical microscopy: relation to corrosion rate. *J. Nucl. Mater.* 2004;324:6–22.
75. Garzarolli F, Seidel H, Tricot R, Gros J. Oxide Growth Mechanism on Zirconium Alloys. In: Eucken C, Garde A, eds. *Zirconium in the Nuclear Industry: Ninth International Symposium*. ASTM International; 1991:STP1132-EB .
76. Platt P, Polatidis E, Frankel P, et al. A study into stress relaxation in oxides formed on zirconium alloys. *J. Nucl. Mater.* 2015;456:415–425.
77. Swan H, Blackmur MS, Hyde JM, et al. The measurement of stress and phase fraction distributions in pre and post-transition Zircaloy oxides using nano-beam synchrotron X-ray diffraction. *J. Nucl. Mater.* 2016;479:559–575.
78. Pétigny N, Barberis P, Lemaignan C, Valot C, Lallemant M. In situ XRD analysis of the oxide layers formed by oxidation at 743 K on Zircaloy 4 and Zr–1NbO. *J. Nucl. Mater.* 2000;280:318–330.
79. Valot C, Ciosmak D, Mesnier MT, Lallemant M. Phase analysis by variable-incidence X-ray diffraction: Application to zirconium oxidation. *Oxid. Met.* 1997;48:329–345.
80. Ni N, Hudson D, Wei J, et al. How the crystallography and nanoscale chemistry of the metal/oxide interface develops during the aqueous oxidation of zirconium cladding alloys. *Acta Mater.* 2012;60:7132–7149.
81. Nicholls RJ, Ni N, Lozano-Perez S, et al. Crystal Structure of the ZrO Phase at Zirconium/Zirconium Oxide Interfaces. *Adv. Eng. Mater.* 2015;17:211–215.
82. Puchala B, Van der Ven A. Thermodynamics of the Zr-O system from first-principles calculations. *Phys. Rev. B*. 2013;88:094108.
83. Vincent B, Optasanu V, Herbst F, et al. Comparison Between the Oxidation Behaviors of Ti6242S, Ti6246, TiXT Alloys, and Pure Titanium. *Oxid. Met.* 2021;96:283–294.
84. Pérez P. Influence of nitriding on the oxidation behaviour of titanium alloys at 700°C. *Surf. Coat. Technol.* 2005;191:293–302.
85. Janek J. Oscillatory kinetics at solid/solid phase boundaries in ionic crystals. *Solid State Ion.* 2000;131:129–142.
86. Valot C, Ciosmak D, Lallemant M. Morphological characteristics of the oxidation of niobium II: The role of stresses on high-temperature morphologies. *Oxid. Met.* 1994;41:235–250.
87. Gibbs GB, Hales R. The influence of metal lattice vacancies on the oxidation of high temperature materials. *Corros. Sci.* 1977;17:487–507.
88. Ni N, Lozano-Perez S, Jenkins ML, et al. Porosity in oxides on zirconium fuel cladding alloys, and its importance in controlling oxidation rates. *Scr. Mater.* 2010;62:564–567.
89. Salazar JM, Lallemant M. Non Linearities In Oxidation Of Metals. *J. Mech. Behav. Mater.* 1994;5:247–260.
90. Lallemant M, Bertrand G, Cannot JC, Larpin JP, Roudergues N, Assire M. Chemical bistability with thermal feedback effect in the oxidation of titanium-43 wt.-% zirconium alloy. *React. Solids*. 1987;3:227–239.
91. Gupta I, Barber JR, Thouless MD, Lu W. Influence of the Turing instability on the motion of domain boundaries. *Phys. Rev. E*. 2020;102:012802.
92. Unnam J, Shenoy RN, Clark RK. Oxidation of commercial purity titanium. *Oxid. Met.* 1986;26:231–252.
93. Clenny JT, Rosa CJ. Oxidation kinetics of niobium in the temperature range of 873 to 1083 K. *Metall. Trans. A*. 1980;11:1385–1389.
94. Waldner P, Eriksson G. Thermodynamic modelling of the system titanium-oxygen. *Calphad*. 1999;23:189–218.
95. Kofstad P. High-temperature oxidation of titanium. *J. Less-Common Met.* 1967;12:449–464.
96. Massih AR, Pérez RJ. *Thermodynamic evaluation of the Nb-O system*. Uppsala, Sweden: Quantum Technologies AB; 2006.
97. Seybolt AU. Solid Solubility of Oxygen In Columbium. *JOM*. 1954;6:774–776.

98. Gebauer J, Franke P, Seifert HJ. Thermodynamic Evaluation of the system Ta–O and Preliminary Assessment of the Systems Al–Nb–O and Al–Ta–O. *Adv. Eng. Mater.* 2022;24:2200162.
99. Dong Y, Motta AT, Marquis EA. Atom probe tomography study of alloying element distributions in Zr alloys and their oxides. *J. Nucl. Mater.* 2013;442:270–281.
100. Lu G, Bernasek SL, Schwartz J. Oxidation of a polycrystalline titanium surface by oxygen and water. *Surf. Sci.* 2000;458:80–90.
101. Ding W, Wang Z, Chen G, et al. Oxidation behavior of low-cost CP-Ti powders for additive manufacturing *via* fluidization. *Corros. Sci.* 2021;178:109080.
102. Sanz JM, Hofmann S. Auger electron spectroscopy and X-ray photoelectron spectroscopy studies of the oxidation of polycrystalline tantalum and niobium at room temperature and low oxygen pressures. *J. Less-Common Met.* 1983;92:317–327.
103. Li R, Álvarez G, Ipakchi A, et al. Understanding the oxidation of pure tungsten in air and its impact on the lifecycle of a fusion power plant. *Nucl. Mater. Energy*. 2025;45:101988.
104. Wang X, Zhao Y, Cui Y, et al. Evolution of fatigue-induced cracks in Cr-coated Zr alloy cladding in high-temperature steam environment. *Corros. Sci.* 2026;263:113722.
105. Amano S, Bogdanovski D, Yamane H, Terauchi M, Dronskowski R. ε-TiO, a Novel Stable Polymorph of Titanium Monoxide. *Angew. Chem.* 2016;128:1684–1689.
106. Wallwork GR, Jenkins AE. Oxidation of Titanium, Zirconium, and Hafnium. *J. Electrochem. Soc.* 1959;106:10.
107. de Castro IA, Datta RS, Ou JZ, et al. Molybdenum Oxides – From Fundamentals to Functionality. *Adv. Mater.* 2017;29:1701619.
108. Couet A, Motta AT, Ambard A. The coupled current charge compensation model for zirconium alloy fuel cladding oxidation: I. Parabolic oxidation of zirconium alloys. *Corros. Sci.* 2015;100:73–84.
109. Douglass DL. *Corrosion mechanism of zirconium and its alloys–diffusion of oxygen in zirconium dioxide*. General Electric Co. Vallecitos Atomic Lab., San Jose, Calif.; 1962.
110. Tsuji T, Shimotani H. Effect of oxygen partial pressure on oxidation of Zr and Zr-2.5wt% Nb alloy. In: Mizutani N, Akashi K, Kimura T, et al., eds. *Advanced Materials '93*. Elsevier; 1994:121–124.
111. Okamoto H. O-Ti (Oxygen-Titanium). *J. Phase Equilibria Diffus.* 2011;32:473–474.
112. Suzuki M, Kawasaki S. Oxidation of zircaloy cladding in air. *J. Nucl. Mater.* 1986;140:32–43.
113. Yoo H-I, Koo B-J, Hong J-O, Hwang I-S, Jeong Y-H. A working hypothesis on oxidation kinetics of Zircaloy. *J. Nucl. Mater.* 2001;299:235–241.
114. García EA. Dynamical diffusion model to simulate the oxide crystallization and grain growth during oxidation of zirconium at 573 and 623 K. *J. Nucl. Mater.* 1995;224:299–304.
115. El Kadiri H, Utegulov ZN, Khafizov M, et al. Transformations and cracks in zirconia films leading to breakaway oxidation of Zircaloy. *Acta Mater.* 2013;61:3923–3935.
116. Salazar JM, Lallemant M. Periodic behaviour in heterogeneous chemical reactions. *Solid State Ion.* 1992;50:233–240.
117. Pérez P, Haanappel VAC, Stroosnijder MF. The effect of niobium on the oxidation behaviour of titanium in N2/20% O2 atmospheres. *Mater. Sci. Eng. A*. 2000;284:126–137.
118. Pérez P, Salmi G, Muñoz A, Monge MA. Influence of yttria additions on the oxidation behaviour of titanium prepared by powder metallurgy. *Scr. Mater.* 2009;60:1008–1011.
119. Gautier K, Epifano E, Gheno T, Connétable D, Monceau D. Effects of Al and refractory alloying elements (W, Ta and Hf) on oxidation kinetics, oxygen dissolution and diffusion in titanium alloys. *Corros. Sci.* 2024;237:112330.
120. Chaze AM, Coddet C. Influence of alloying elements on the dissolution of oxygen in the metallic phase during the oxidation of titanium alloys. *J. Mater. Sci.* 1987;22:1206–1214.
121. Valenza TC, Chao P, Weber PK, Neill OK, Marquis EA. Protective role of silicon in the high-temperature oxidation of titanium. *Corros. Sci.* 2023;217:111110.
122. Rosa CJ. Oxidation of Ti-1Si and Ti-5Si alloys. *Oxid. Met.* 1982;17:359–369.
123. Shu J, Dong Z, Zheng C, et al. High-throughput experiment-assisted study of the alloying effects on oxidation of Nb-based alloys. *Corros. Sci.* 2022;204:110383.
124. Zhang S-N, Jia L-N, Guo Y-L, Kong B, Zhang F-X, Zhang H. High-temperature oxidation behavior of Nb–Si-based alloy with separate vanadium, tantalum, tungsten and zirconium addition. *Rare Met.* 2021;40:607–615.
125. Geng J, Tsakiropoulos P, Shao G. A thermo-gravimetric and microstructural study of the oxidation of Nbss/Nb5Si3-based *in situ* composites with Sn addition. *Intermetallics*. 2007;15:270–281.
126. Li J, Chen Y, Li Y, Bai Z, Wang K. Influence of aluminium addition on oxidation resistance of Ta-W alloy. *Powder Metall.* 2019;62:322–330.

127. Liu D, Zheng L, Luo L, et al. An overview of oxidation-resistant tungsten alloys for nuclear fusion. *J. Alloys Compd.* 2018;765:299–312.
128. Zhang W, Qi Y, Zhang L, et al. The effect of alloy elements on corrosion and oxidative resistance of W-based alloy films. *Surf. Coat. Technol.* 2022;434:128165.
129. Kanjer A, Optasanu V, Lavisse L, et al. Influence of Mechanical Surface Treatment on High-Temperature Oxidation of Pure Titanium. *Oxid. Met.* 2017;88:383–395.
130. Knaislová A, Novák P, Průša F, Cabibbo M, Jaworska L, Vojtěch D. High-temperature oxidation of Ti–Al–Si alloys prepared by powder metallurgy. *J. Alloys Compd.* 2019;810:151895.
131. Raceanu L, Optasanu V, Montesin T, Montay G, François M. Shot-Peening of Pre-Oxidized Plates of Zirconium: Influence of Residual Stress on Oxidation. *Oxid. Met.* 2013;79:135–145.
132. Hennessey TP, Morral JE. Oxidation and nitridation of niobium in air above 1150°C. *Oxid. Met.* 1992;38:163–187.
133. Borcz C, Lepienski CM, Brunatto SF. Surface modification of pure niobium by plasma nitriding. *Surf. Coat. Technol.* 2013;224:114–119.
134. Schlueter K, Balden M. Dependence of oxidation on the surface orientation of tungsten grains. *Int. J. Refract. Met. Hard Mater.* 2019;79:102–107.
135. Bartlett RW, McCamont JW. The influence of crystal orientation on the oxidation of tungsten. *J. Electrochem. Soc.* 1965;112:148.
136. Gorsse S, Miracle DB, Senkov ON. Mapping the world of complex concentrated alloys. *Acta Mater.* 2017;135:177–187.
137. Senkov ON, Scott JM, Senkova SV, Miracle DB, Woodward CF. Microstructure and room temperature properties of a high-entropy TaNbHfZrTi alloy. *J. Alloys Compd.* 2011;509:6043–6048.
138. Wang S, Wu M, Shu D, Zhu G, Wang D, Sun B. Mechanical instability and tensile properties of TiZrHfNbTa high entropy alloy at cryogenic temperatures. *Acta Mater.* 2020;201:517–527.
139. Senkov ON, Scott JM, Senkova SV, Meisenkothen F, Miracle DB, Woodward CF. Microstructure and elevated temperature properties of a refractory TaNbHfZrTi alloy. *J. Mater. Sci.* 2012;47:4062–4074.
140. Anber EA, Beaudry D, Brandenburg C, et al. Oxidation resistance of Al-containing refractory high-entropy alloys. *Scr. Mater.* 2024;244:115997.
141. Ghadyani M, Utton C, Tsakiropoulos P. Microstructures and Isothermal Oxidation of the Alumina Scale Forming Nb1.7Si2.4Ti2.4Al3Hf0.5 and Nb1.3Si2.4Ti2.4Al3.5Hf0.4 Alloys. *Materials*. 2019;12:222.
142. Lo K-C, Murakami H, Yeh J-W, Yeh A-C. Oxidation behaviour of a novel refractory high entropy alloy at elevated temperatures. *Intermetallics*. 2020;119:106711.
143. Schellert S, Gorr B, Laube S, Kauffmann A, Heilmaier M, Christ HJ. Oxidation mechanism of refractory high entropy alloys Ta-Mo-Cr-Ti-Al with varying Ta content. *Corros. Sci.* 2021;192:109861.
144. Schofield T, Bacon A. Ti-O Phase Diagram. *JOM*. 1955;84:47.
145. Gebhardt E, Seghezzi H-D, Dürrschnabel W. Untersuchungen in system Zirkonium-Sauerstoff teil 2 untersuchungen zur kinetik der reaktion zwischen Zirkonium und sauerstoff, sowie über die konstitution des systems Zirkonium-Sauerstoff. *J. Nucl. Mater.* 1961;4:255–268.
146. Sheikh S, Bijaksana MK, Motallebzadeh A, et al. Accelerated oxidation in ductile refractory high-entropy alloys. *Intermetallics*. 2018;97:58–66.
147. *Corrosion: Materials*. ASM International; 2005.
148. Maier HJ, Niendorf T, Bürgel R. *Handbuch Hochtemperatur-Werkstofftechnik: Grundlagen, Werkstoffbeanspruchungen, Hochtemperaturlegierungen und -beschichtungen*. Wiesbaden: Springer Fachmedien; 2019.
149. Müller F, Gorr B, Christ H-J, et al. On the oxidation mechanism of refractory high entropy alloys. *Corros. Sci.* 2019;159:108161.
150. Jehn H, Olzi E. High temperature solid-solubility limit and phase studies in the system tantalum-oxygen. *J. Less-Common Met.* 1972;27:297–309.
151. Meyer MK, Thom AJ, Akinc M. Oxide scale formation and isothermal oxidation behavior of Mo–Si–B intermetallics at 600–1000°C. *Intermetallics*. 1999;7:153–162.
152. Birks N, Meier GH, Pettit FS. *Introduction to the High Temperature Oxidation of Metals*. Cambridge University Press; 2006.
153. Zhang K, Zhao Y, Li J, et al. High-temperature steam corrosion performance of FeCrAl alloys after long-term service in PWR condition: A reliable evaluation and multiscale microstructural characterization. *Corros. Sci.* 2026;264:113747.